Supplement of

The Role of Naphthalene and Its Derivatives in the Formation of Secondary Organic Aerosols in the Yangtze River Delta Region, China

Fei Ye et al.

Correspondence to: Jingyi Li (jingyili@nuist.edu.cn), Jianlin Hu (jianlinhu@nuist.edu.cn)

Contents of this file:

Text S1-S2

Table S1-S5

Figures S1-S9

References

Text S1. Fitting the SOA yield by one-product and two-product methods

In the CMAQ model, counter species were used to calculate the production of SOA through gas-particle partitioning based on yields (α_i) and partitioning coefficients ($K_{\text{om},i}$, m³ µg⁻¹) of condensable organic products derived from chamber experiment data. The definition of $K_{\text{om},i}$ followed Pankow (1994) as shown below:

$$K_{\text{om, }i} = \frac{1}{C_{\text{sat},i}^*} = \frac{RT}{10^6 \overline{\text{MW}_{\text{om}}} \xi_i P_{\text{L},i}^0} \tag{1}$$

where $\overline{\text{MW}_{\text{om}}}$ (g mol⁻¹) is the average molecular weight of the organic phase, ξ_i is the activity coefficient of species I in the absorbing organic phase, $P_{\text{L},i}^0$ (atm) is the vapor pressure of species I at temperature T (K), and R (8.314 J mol⁻¹ K⁻¹) is the gas constant. Factor 10^6 is needed for unit conversion. The inverse of the saturation concentration of species i, $C_{\text{sat},i}^*$ (µg m⁻³), is equivalent to $K_{\text{om},i}$. The temperature dependence of $C_{\text{sat},i}^*$ was calculated by the Clausius–Clapeyron equation (Hayes et al., 2015):

$$C_{\text{sat, }i}^* = C_{0,i}^* \frac{T_0}{T} \exp\left[\frac{\Delta H_{\text{vap},i}}{R}\left(\frac{1}{T_0} - \frac{1}{T}\right)\right] \tag{2}$$

where $C_{0,i}^*$ is the effective saturation concentration of condensable species i at the reference temperature T_0 (K), usually taken as 298 K. $\Delta H_{\text{vap},i}$ (J mol⁻¹) is the enthalpy of vaporization.

Assuming that the condensable organic products are P_1, P_2,…P_n, the total SOA yield (Y) of a certain parent VOC was calculated as follows (Odum et al., 1996):

$$Y = \sum_i Y_i = M_0 \sum_i \frac{\alpha_i K_{\text{om},i}}{1 + M_0 K_{\text{om},i}} \tag{3}$$

where α_i is the mass-based stoichiometric coefficient of semi-volatile product i. M_0 is the total mass concentration of the absorbing aerosol medium. The SOA formation scheme is named the n-product method based on the total number (n) of P_i. Accordingly, the total SOA yield of the two-product and one-product methods can be derived as follows:

$$Y = \frac{\alpha_1}{1 + \dfrac{1}{M_0 K_{om,1}}} + \frac{\alpha_2}{1 + \dfrac{1}{M_0 K_{om,2}}} \tag{4}$$

$$Y = \frac{\alpha_1}{1 + \dfrac{1}{M_0 K_{om,1}}} \tag{5}$$

Text S2. Estimation of MN emissions

To obtain the detailed emissions of 1-MN and 2-MN, the ratios of 1-MN/2MN to non-methane volatile organic compounds (NMVOCs) of different sources were calculated as follows:

$$p = \sum_{i=1}^{n} (a_i * W_i) \tag{6}$$

where p is the mass proportion of 1-MN/2-MN to total NMVOC emissions in a major source, a_i is the mass ratio of 1-MN/2-MN to NMVOCs in a subcategorized source i, and W_i is the weight percent of the total emitted NMVOCs from a subcategorized source i to that of the major source. For a specific source i, a_i was obtained from the US EPA (Environmental Protection Agency) repository of organic gas and PM speciation profiles of air pollution sources (SPECIATEv5.2), and W_i was based on the information reported by An et al. (2021) for the YRD and Li et al. (2014) for other regions, respectively.

Table S1. The yield (α), equilibrium partitioning coefficient (K_{om}), and enthalpy of SOA precursors from Nap, 1-MN, and 2-MN.

	Species	α_1	$K_{om,\ 1}$ (m^3 µg^{-1})	α_2	$K_{om,\ 2}$ (m^3 µg^{-1})	Enthalpy (kJ mol^{-1})	References for α and C_{star}
High NO$_x$	Nap	0.210	0.602	1.07	3.77E-3	18	CMAQ
(one-product)	1-MN	0.500	0.110	-	-	16.6	Chan et al. (2009)
	2-MN	0.550	0.130	-	-	17.5	Chan et al. (2009)
High NO$_x$	Nap	0.210	0.602	1.07	3.77E-3	18	CMAQ
(two-product)	1-MN	0.206	0.193	0.107	0.001	16.6	Shakya and Griffin (2010)
	2-MN	0.247	0.193	0.0920	0.001	17.5	Shakya and Griffin (2010)
Low NO$_x$	Nap	0.730	[a]				CMAQ
	1-MN	0.680	[a]				Chan et al. (2009)
	2-MN	0.580	[a]				Chan et al. (2009)

[a] Constant yield

Table S2. Sector-based mass ratios of Nap, 1-MN, and 2-MN to NMVOC emissions in the emis-orig case.

Emission region	Species	residential	road transport	industry	industrial solvent use	residential solvent use	wildfire[c]
YRD region[a]	Nap	The original Nap emission in YRD					0.391
	1-MN	0.0739	0.0143	2.62E-3	5.47E-4	0.0115	0.134
	2-MN	0.0898	0.0232	0.0116	2.38E-3	0.0500	0.170
	Species	residential	transportation	industry	power	agriculture	wildfire[c]
Other regions[b]	Nap	0.0252	0.0317	0.0983	-	-	0.391
	1-MN	3.95E-3	4.38E-3	1.67E-4	-	-	0.134
	2-MN	0.0108	7.24E-3	1.11E-3	-	-	0.170

[a] The YRD inventory was used for the YRD region and was divided into 13 sources (ship, nonroad transport, road transport, industry, industrial solvent use, residential solvent use, agriculture, residential, industry boiler and kiln, power, dust, oil storage and transportation, gasoline vehicle evaporative emissions), among which only sources with none zero mass ratios of Nap and MN were listed in the Table. [b] The MEIC inventory was used for other regions and was divided into 5 sources. [c] The ratios of Nap and MN for wildfire emissions in the YRD region were the same as in other regions.

Table S3. Settings of all the scenarios.

Case	Emission setting	SOA parameterization for MN
base1	Set emissions of Nap and MN to zero based on the emis-adjust	one-product method
case-1product-orig	Use the original Nap emissions from the 2017 YRD inventory	one-product method
case-2products-orig	and new-added MN emissions (emis-orig)	two-product method
case-1product	The anthropogenic emissions of Nap and MN in the YRD	one-product method
case-2products	region from emis-orig were multiplied by 5 and 7, respectively, and unchanged in other regions (emis-adjust)	two-product method

Table S4. Model performance of MDA8 O_3 and daily average $PM_{2.5}$, SO_2, NO_2, and CO in several cities listed in Fig. S2 in case-1product. OBS and PRE represent observation and prediction concentrations, respectively. The benchmarks follow Emery et al. (2017). Performances exceeding the benchmark are represented in bold font.

Species	Metrics	Suzhou	Nanjing	Hangzhou	Hefei	Shanghai	Benchmark
MDA8	OBS	68.37	75.22	70.74	71.29	65.85	
O_3 (ppb)	PRE	71.54	71.93	73.49	68.48	47.50	
	NMB	0.05	-0.04	0.04	-0.04	-0.28	<±0.15
	NME	0.25	0.17	0.22	0.23	0.33	<0.25
	R	0.40	0.73	0.62	0.56	0.25	
$PM_{2.5}$	OBS	42.16	38.41	37.65	46.54	42.04	
($\mu g\ m^{-3}$)	PRE	31.83	36.79	31.91	48.53	23.99	
	NMB	-0.24	-0.04	-0.15	0.04	-0.43	<±0.30
	NME	0.33	0.26	0.39	0.32	0.47	<0.50
	R	0.36	0.39	0.21	0.38	0.47	
SO_2	OBS	2.33	3.42	3.03	2.50	3.80	
(ppb)	PRE	2.51	3.55	2.36	2.70	1.76	
	NMB	0.08	0.04	-0.22	0.08	-0.54	
	NME	0.35	0.20	0.24	0.36	0.54	
	R	0.49	0.70	0.64	0.50	0.44	

NO$_2$	OBS	18.77	17.84	18.54	19.80	17.34
(ppb)	PRE	12.56	13.84	10.92	15.03	17.57
	NMB	-0.33	-0.22	-0.41	-0.24	0.01
	NME	0.34	0.24	0.41	0.25	0.18
	R	0.49	0.67	0.33	0.83	0.83
CO	OBS	549.52	590.07	673.79	644.89	495.34
(ppb)	PRE	471.97	611.71	483.32	507.03	307.43
	NMB	-0.14	0.04	-0.28	-0.21	-0.38
	NME	0.26	0.17	0.30	0.25	0.39
	R	0.73	0.68	0.36	0.50	0.78

Table S5. Model performance of daily ARO1, ARO2MN', BENZ, NO$_2$, and NO at the Taizhou site in case-1product. The units of OBS (observation) and PRE (prediction) are ppb.

	ARO1	ARO2MN'	BENZ	NO$_2$	NO
OBS	0.05	0.37	0.52	9.13	1.42
PRE	0.71	0.45	0.61	7.25	0.96
NMB	13.20	0.23	0.19	-0.21	-0.32
NME	13.20	0.36	0.37	0.27	0.62
r	0.80	0.77	0.75	0.79	0.16
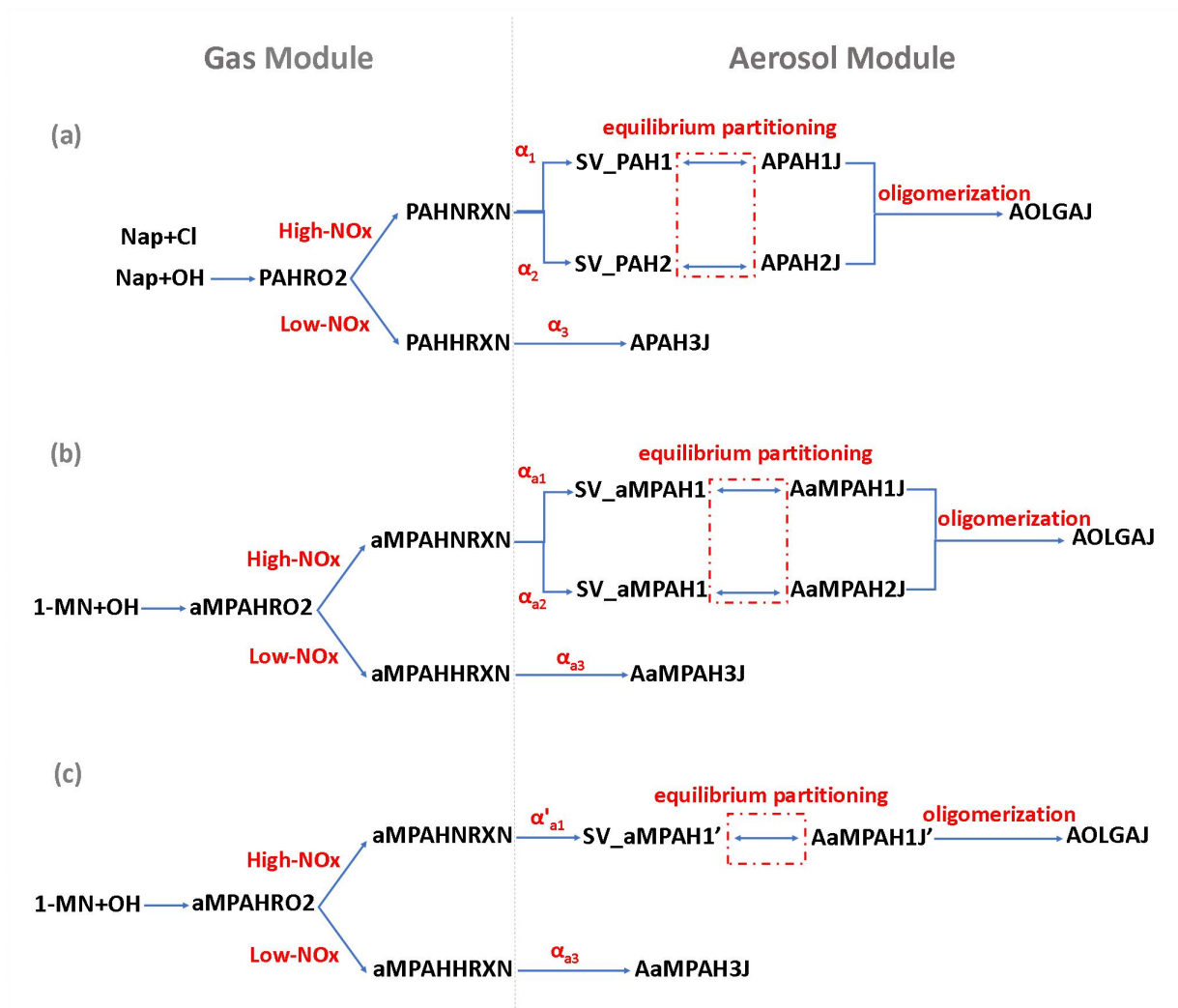
Figure S1. Scheme of SOA module in CMAQv5.2. (a) pre-existing SOA formation pathways for Nap fitted by two products under high NO$_x$; (b) newly added SOA formation pathways for 1-MN fitted by two products under high NO$_x$; (c) newly added SOA formation pathways for 1-MN fitted by one product under high NO$_x$. The values of α refer to Table S1.
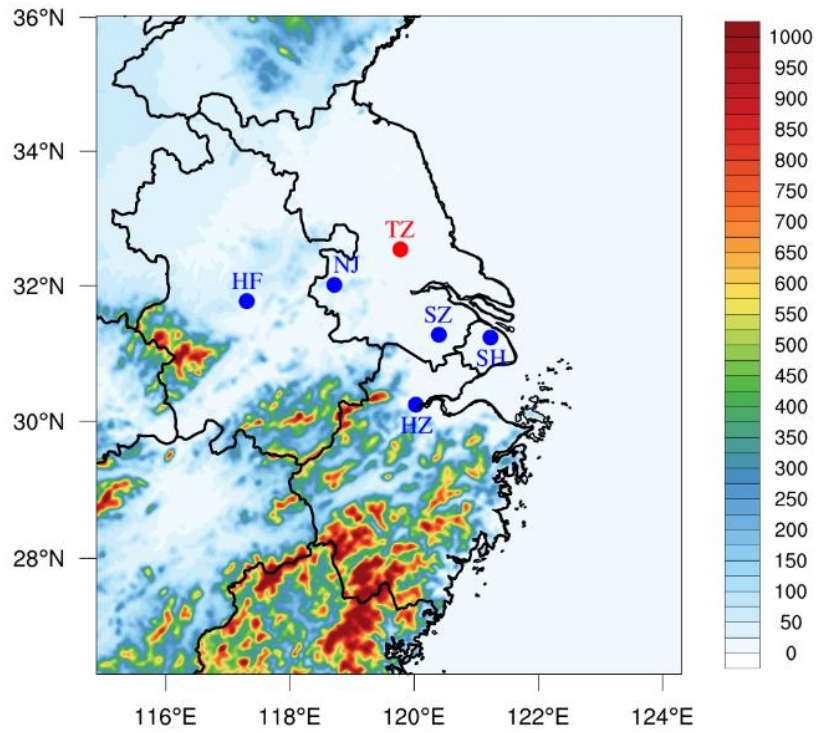
Figure S2. The modeling domain and locations of Taizhou city (red dot) and other sites (Hefei, Nanjing, Suzhou, Shanghai, and Hangzhou; blue dots) for model performance evaluation. The color bar on the right represents the topography height (in meters).
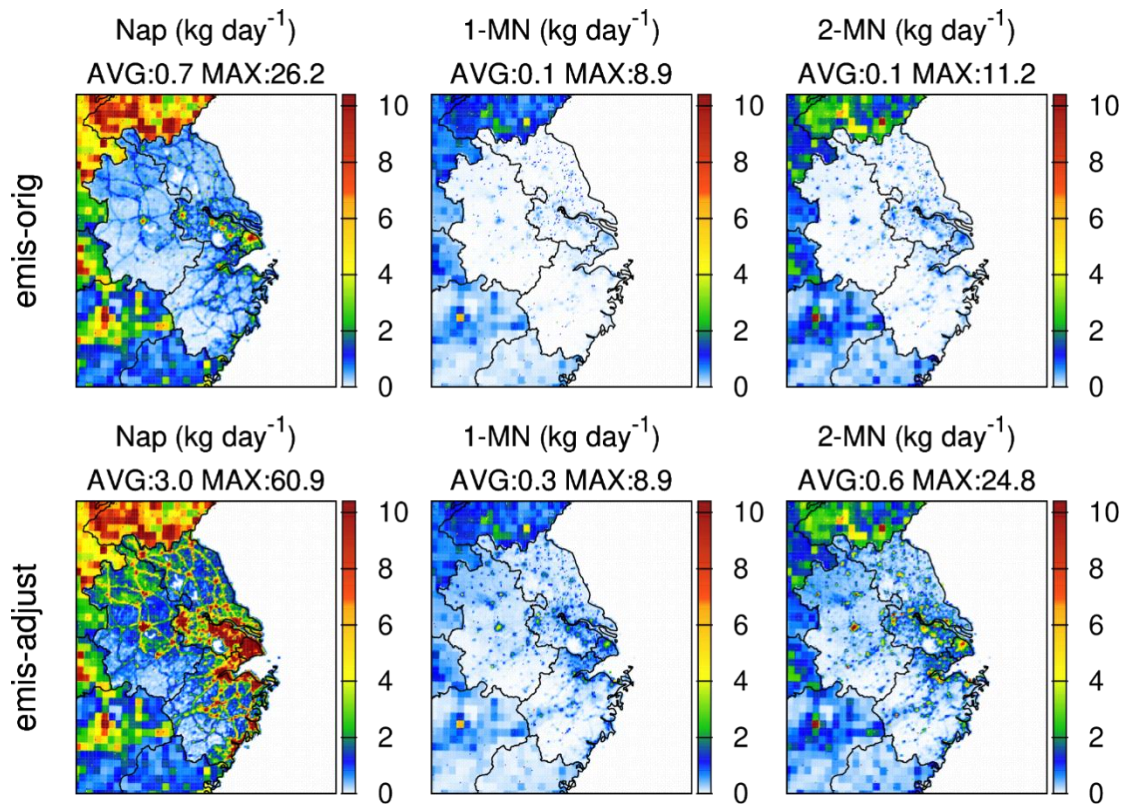
Figure S3. Regional distributions of Nap, 1-MN, and 2-MN emissions in emis-orig and emis-adjust.
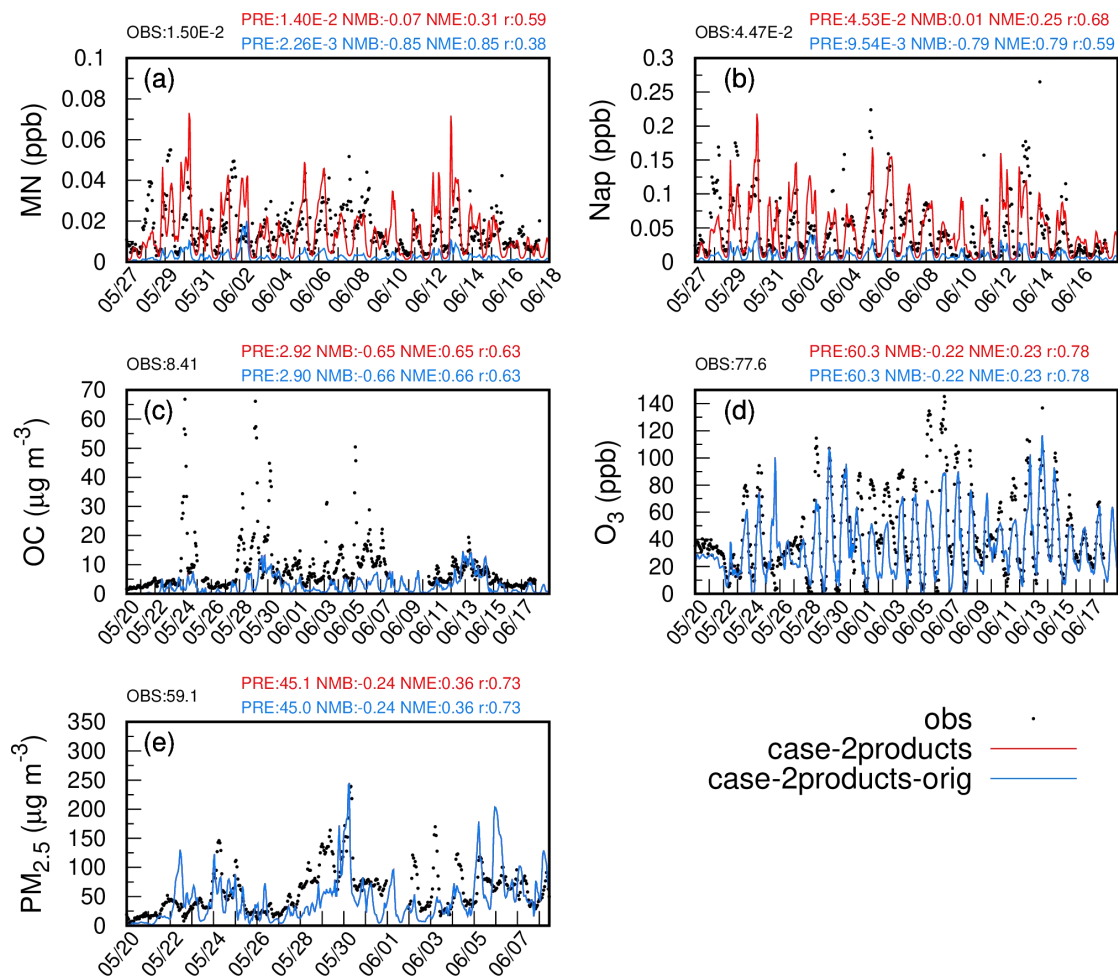
Figure S4. Observed and simulated hourly concentrations of MN, Nap, OC, PM₂.₅, and O₃ based on emis-adjust (red) and emis-orig (blue) at the Taizhou site. Model performances of daily MN, Nap, OC, PM₂.₅, and MDA8 O₃ are shown in blue for case-2products-orig and red for case-2products. OBS and PRE represent averaged concentrations of observations and predictions, respectively.
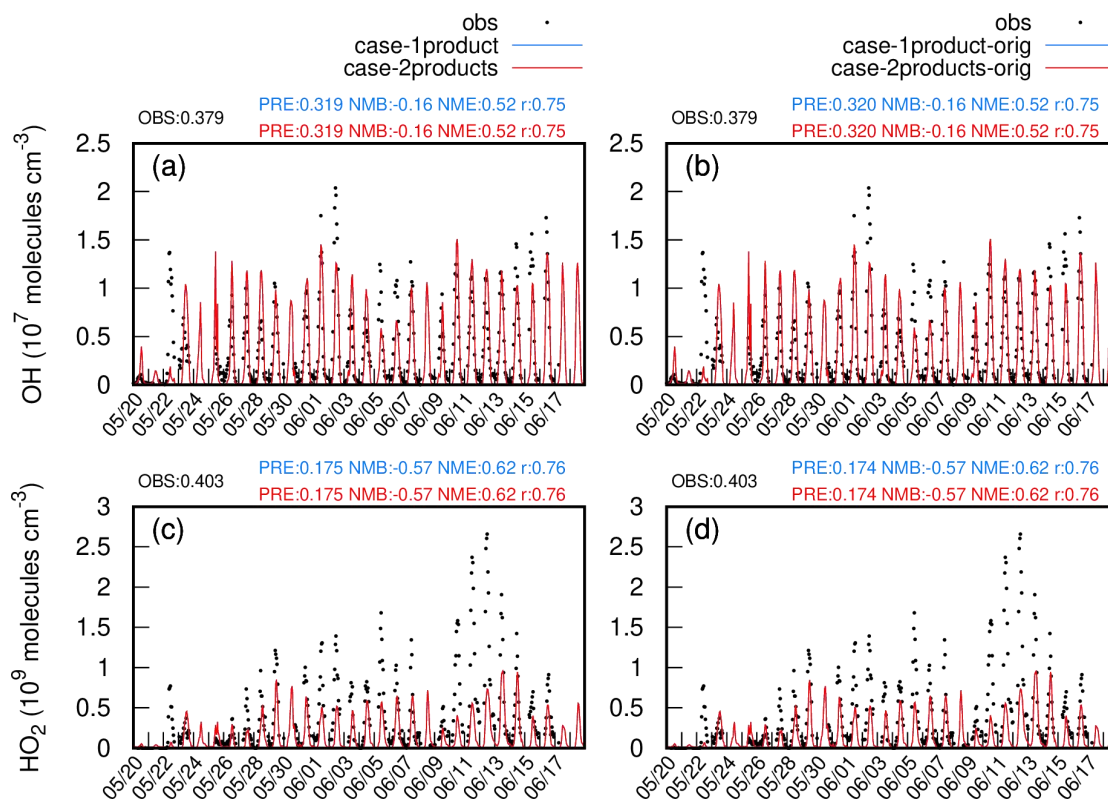
Figure S5. Observed and predicted temporal variations of OH and HO$_2$ radicals based on emis-adjust (left column) and emis-orig (right column) at the Taizhou site. Model performances of OH and HO$_2$ radicals are shown in blue for case-1product or case-1product-YRD and red for case-2products or case-2products-YRD when compared with the observations from the EXPLORE-YRD campaign. OBS and PRE represent the average of observation and prediction, respectively.
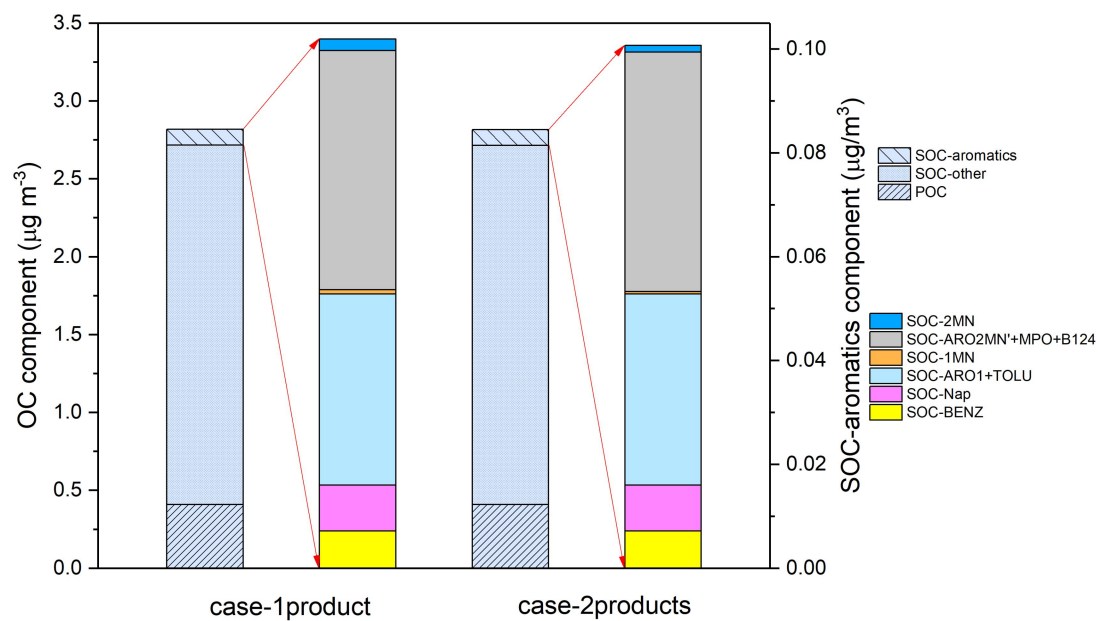
Figure S6. Episode-averaged composition of OC and SOC-aromatics in case-1product and case-2products. SOC-aromatics represent the SOC generated by all the aromatic precursors. SOC-other represents SOC minus SOC-aromatics.
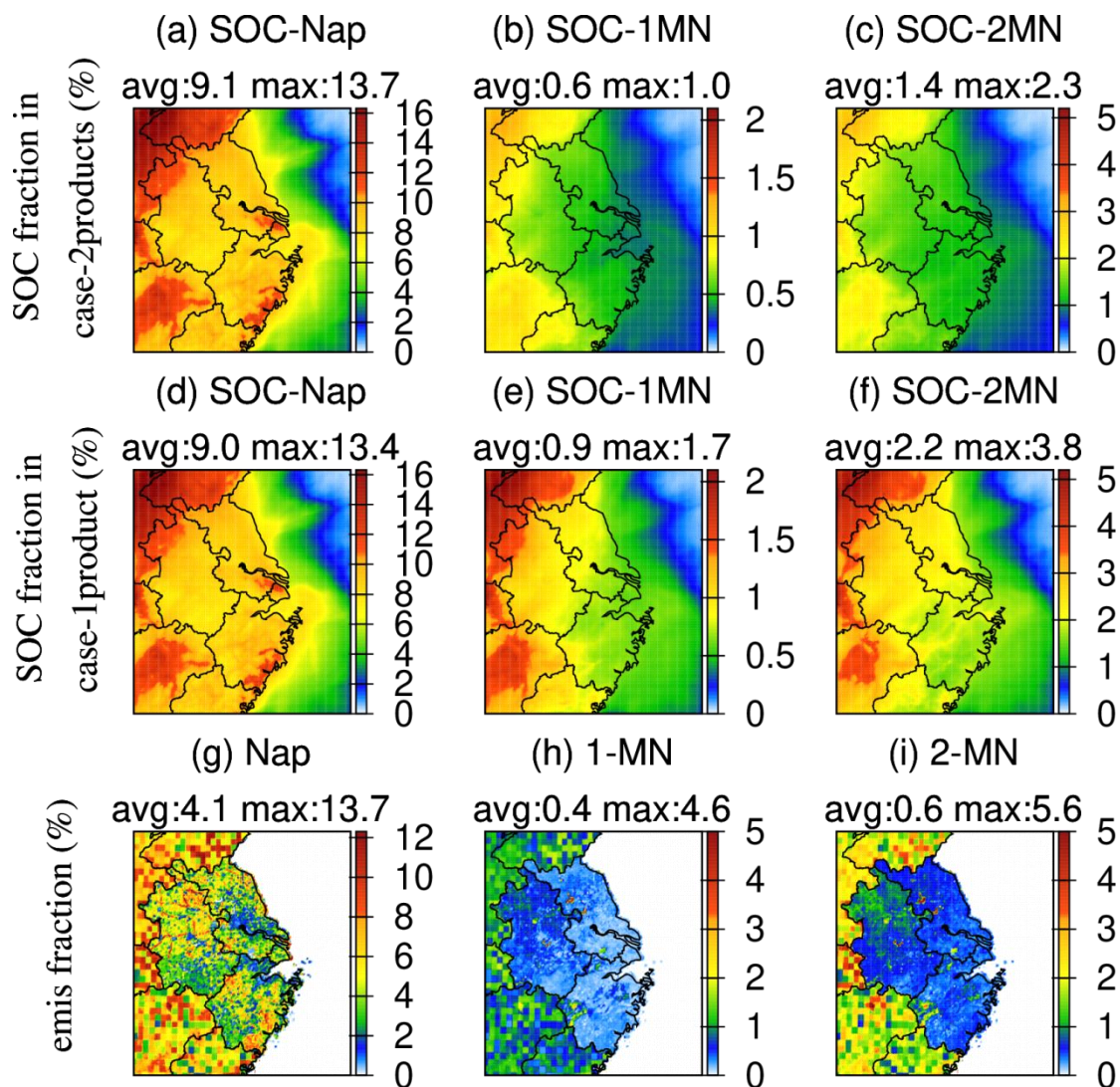
Figure S7. Contributions of Nap, 1-MN, and 2-MN to aromatic-derived SOC in the case-2products (a–c) and the case-1product (d–f) and to the total aromatic emissions (g–i).
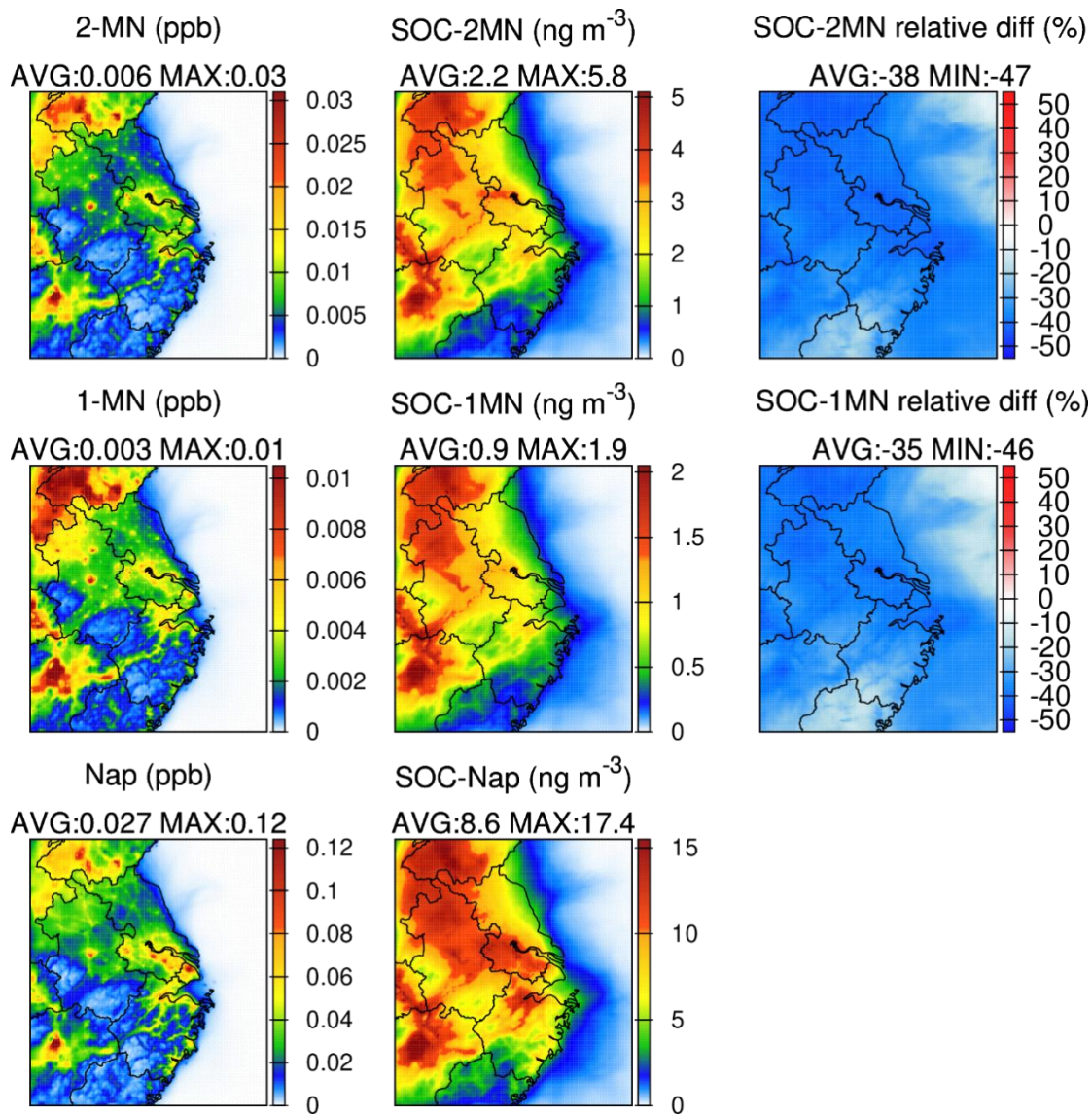
Figure S8. Episode-averaged concentrations of Nap, 1-MN, and 2-MN in case-1product (first column), concentrations of SOC-Nap, SOC-1MN, and SOC-2MN in case-1product (second column), and relative differences of SOC-1MN and SOC-2MN between case-2products and case-1product calculated as (case-2products - case-1product)/ case-1product×100 % (third column).
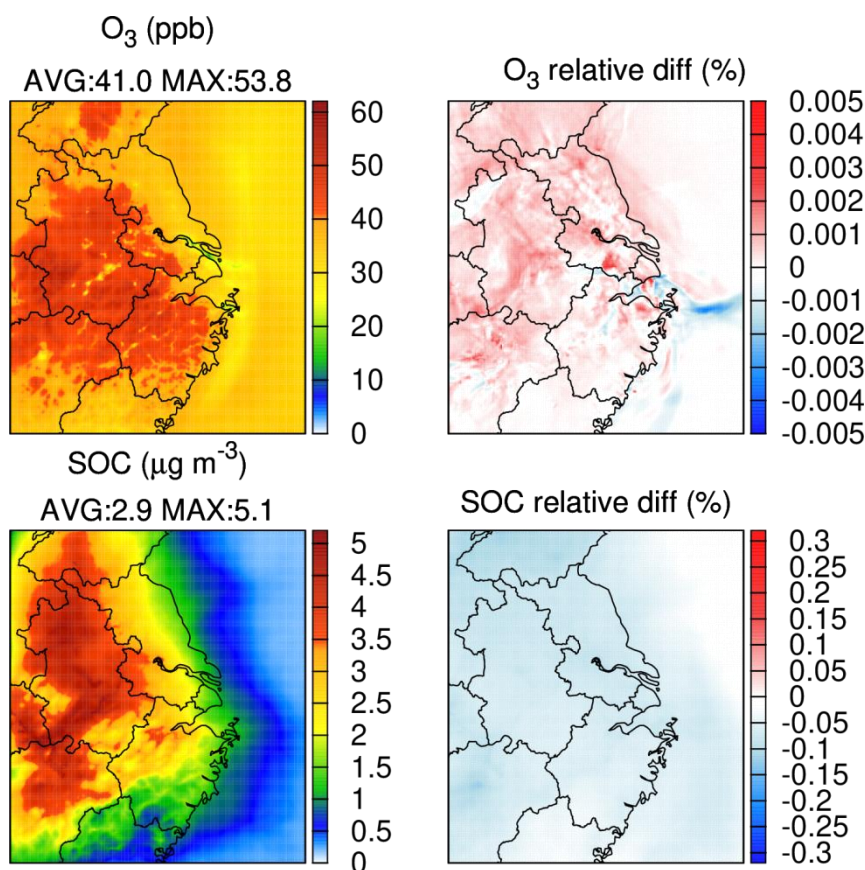
Figure S9. Episode-averaged concentrations of SOC and O_3 in case-1product (left column) and the changes of O_3 and SOC in case-2products relative to case-1product (right column).

References

An, J., Huang, Y., Huang, C., Wang, X., Yan, R., Wang, Q., Wang, H., Jing, S. a., Zhang, Y., Liu, Y., Chen, Y., Xu, C., Qiao, L., Zhou, M., Zhu, S., Hu, Q., Lu, J., and Chen, C.: Emission inventory of air pollutants and chemical speciation for specific anthropogenic sources based on local measurements in the Yangtze River Delta region, China, Atmospheric Chemistry and Physics, 21, 2003-2025, 10.5194/acp-21-2003-2021, 2021.

Chan, A. W. H., Kautzman, K. E., Chhabra, P. S., Surratt, J. D., Chan, M. N., Crounse, J. D., Kürten, A., Wennberg, P. O., Flagan, R. C., and Seinfeld, J. H.: Secondary organic aerosol formation from photooxidation of naphthalene and alkylnaphthalenes: implications for oxidation of intermediate volatility organic compounds (IVOCs), Atmos. Chem. Phys., 9, 3049-3060, 10.5194/acp-9-3049-2009, 2009.

Emery, C., Liu, Z., Russell, A. G., Odman, M. T., Yarwood, G., and Kumar, N.: Recommendations on statistics and benchmarks to assess photochemical model performance, J Air Waste Manag Assoc,

67, 582-598, 10.1080/10962247.2016.1265027, 2017.

Hayes, P. L., Carlton, A. G., Baker, K. R., Ahmadov, R., Washenfelder, R. A., Alvarez, S., Rappenglück, B., Gilman, J. B., Kuster, W. C., de Gouw, J. A., Zotter, P., Prévôt, A. S. H., Szidat, S., Kleindienst, T. E., Offenberg, J. H., Ma, P. K., and Jimenez, J. L.: Modeling the formation and aging of secondary organic aerosols in Los Angeles during CalNex 2010, Atmospheric Chemistry and Physics, 15, 5773-5801, 10.5194/acp-15-5773-2015, 2015.

Li, M., Zhang, Q., Streets, D. G., He, K. B., Cheng, Y. F., Emmons, L. K., Huo, H., Kang, S. C., Lu, Z., Shao, M., Su, H., Yu, X., and Zhang, Y.: Mapping Asian anthropogenic emissions of non-methane volatile organic compounds to multiple chemical mechanisms, Atmos. Chem. Phys., 14, 5617-5638, 10.5194/acp-14-5617-2014, 2014.

Odum, J. R., Hoffmann, T., Bowman, F., Collins, D., Flagan, R. C., and Seinfeld, J. H.: Gas/Particle Partitioning and Secondary Organic Aerosol Yields, Environmental Science & Technology, 30, 2580-2585, 10.1021/es950943+, 1996.

Pankow, J. F.: An absorption model of gas/particle partitioning of organic compounds in the atmosphere, Atmospheric Environment, 28, 185-188, https://doi.org/10.1016/1352-2310(94)90093-0, 1994.

Shakya, K. M. and Griffin, R. J.: Secondary Organic Aerosol from Photooxidation of Polycyclic Aromatic Hydrocarbons, Environmental Science & Technology, 44, 8134-8139, 10.1021/es1019417, 2010.